



**HAL**  
open science

# Learnable Empirical Mode Decomposition based on Mathematical Morphology

Santiago Velasco-Forero, Romain Pagès, Jesus Angulo

► **To cite this version:**

Santiago Velasco-Forero, Romain Pagès, Jesus Angulo. Learnable Empirical Mode Decomposition based on Mathematical Morphology. 2021. hal-03221652v2

**HAL Id: hal-03221652**

**<https://hal.science/hal-03221652v2>**

Preprint submitted on 21 Jul 2021 (v2), last revised 26 Aug 2021 (v3)

**HAL** is a multi-disciplinary open access archive for the deposit and dissemination of scientific research documents, whether they are published or not. The documents may come from teaching and research institutions in France or abroad, or from public or private research centers.

L'archive ouverte pluridisciplinaire **HAL**, est destinée au dépôt et à la diffusion de documents scientifiques de niveau recherche, publiés ou non, émanant des établissements d'enseignement et de recherche français ou étrangers, des laboratoires publics ou privés.

# Learnable Empirical Mode Decomposition based on Mathematical Morphology \*

Santiago Velasco-Forero<sup>†</sup>, R. Pagès<sup>‡</sup>, and Jesus Angulo<sup>§</sup>

**Abstract.** Empirical mode decomposition (EMD) is a fully data driven method for multiscale decomposing signals into a set of components known as intrinsic mode functions. EMD is based on lower and upper envelopes of the signal in an iterated decomposition scheme. In this paper, we put forward a simple yet effective method to learn EMD from data by means of morphological operators. We propose an end-to-end framework by incorporating morphological EMD operators into deeply learned representations, trained using standard backpropagation principle and gradient descent-based optimization algorithms. Three generalizations of morphological EMD are proposed: a) by varying the family of structuring functions, b) by varying the pair of morphological operators used to calculate the envelopes, and c) by considering a convex sum of envelopes instead of the mean point used in classical EMD. We discuss in particular the invariances that are induced by the morphological EMD representation. Experimental results on supervised classification of hyperspectral images by 1D convolutional networks demonstrate the interest of our method.

**Key words.** Deep Learning, Mathematical morphology, Hyperspectral image processing

**AMS subject classifications.** 68U10, 94A12, 68T07

**1. Introduction.** Deep convolutional neural networks (DCNN) provide state-of-the-art results in many tasks for signal and image classification [4]. The DCNN architectures combine low complexity signal/image operators, like convolution with small kernels or pooling estimation, with the ability to optimize the corresponding weights of the operators in evolved and hierarchical networks. Traditional models for signal/image representation and associated feature extraction are generally not compatible with the DCNN paradigm. The main limitation is the incompatibility of the backpropagation principle used to train the parameters of the neural networks by gradient descent algorithms. In the case of traditional signal/image processing, the interpretability of the operators and features is often straightforward. We focus here in particular in the *Empirical Mode Decomposition* (EMD) [24], which is a simple and powerful technique used to represent the features of a signal (without any assumption on its frequency content) from a geometric viewpoint, basically using lower and upper envelopes of the signal in an iterated decomposition. The two main ingredients of EMD: detection of local extrema and the interpolation between them, are not naturally formulated in the neural network paradigm. Inspired by the work of Diop and co-workers [12, 11, 13], we revisit EMD using morphological operators to deal with lower/upper envelopes. Additionally, we propose three generalizations: a) by varying the family of structuring functions, b) by varying the pair of morphological operators used to calculate the envelopes, and c) by considering a convex

\*

**Funding:** This work was funded by the Fondation Jacques Hadamard under PGM0-IRSDI 2019 program.

<sup>†</sup>CMM, MINES ParisTech, PSL Research University, France ([santiago.velasco@mines-paristech.com](mailto:santiago.velasco@mines-paristech.com), <http://cmm.ensmp.fr/~velasco/>).

<sup>‡</sup>École Centrale de Lyon, France ([romain.pages@ecl18.ec-lyon.fr](mailto:romain.pages@ecl18.ec-lyon.fr)).

<sup>§</sup>CMM, MINES ParisTech, PSL Research University, France ([angulo@mines-paristech.com](mailto:angulo@mines-paristech.com), <http://cmm.ensmp.fr/~angulo/>).

36 sum of envelopes instead of the mean point used in classical EMD. All the parameters of our  
 37 proposition can be learnt using backpropagation and gradient descent techniques and therefore  
 38 the associated morphological EMD can be integrated into standard DCNN representations for  
 39 end-to-end learning. The integration of morphological operators into DCNN pipelines is an  
 40 active research area. First attempts were based on approximation of dilation and erosion using  
 41 standard convolution [33]. More recently, straightforward approaches of dilation and erosion  
 42 optimization have been explored [14, 34, 38]. However, plugging morphological operators into  
 43 standard networks is far from being trivial from the optimization based on backpropagation  
 44 of gradients through all layers by the chain rule. Max-plus operators are indeed differentiable  
 45 only on a local and specific domain. Here we focus on standard gradient descent strategies  
 46 and we provide a better understanding of how the gradient of morphological operators, in  
 47 particular those associated to parametric structuring functions, is defined. Additionally, we  
 48 show that our morphological EMD induces the invariance to additive shift in standard DCNN.  
 49 To the best of our knowledge, these technical aspects have not been previously discussed in  
 50 the field of morphological deep neural networks.

51 **1.1. Related work.** In what follows we review the state-of-the-art that is most relevant  
 52 for the proposed morphological EMD.

53 **1.1.1. Empirical Mode Decomposition.** EMD is an algorithm introduced by Huang et al.  
 54 [24] for analysing linear and non-stationary time series. It is a way to decompose a signal in order  
 55 to obtain instantaneous frequency data. In this original version of the EMD is an iterative  
 56 process which decomposes real signals  $f$  into simpler signals (modes),  $f(x) = \sum_{i=1}^M \Phi_j(x)$ ,  
 57 where each *mono-component* signal  $\Phi$  should be written in the form  $\Phi(x) = r(x) \cos(\theta x)$ ,  
 58 where the amplitude and phase are both physically and mathematically meaningful [49]. Un-  
 59 like some other common transforms like the Fourier transform for example, the EMD was  
 60 built as an algorithm and lacks theoretical background then. The problem of EMD to rep-  
 61 resent a signal as a sum of amplitude modulation (AM) and frequency modulation (FM)  
 62 components at multiple scales was first proposed in [32] where the problem of finding the  
 63 AM-FM components and their envelopes was solved using multiscale Gabor filters and non-  
 64 linear Teager-Kaiser Energy Operators via an Energy Separation Algorithm (ESA). In the  
 65 original EMD, there is no parametric family of filters used to estimate the envelopes.

66 From an algorithmic point of view, the EMD is obtained following the iterative process  
 67 [24]:

- 68 1. Find all the local extrema of the function  $f$ .
- 69 2. Interpolate all the local maxima together to get the function  $\hat{f}$  (upper envelope), and  
 70 all the local minima together to get the function  $\check{f}$  (lower envelope)
- 71 3. Calculate the *local mean* as the average of the both interpolations; the obtained func-  
 tion is called *Intrinsic Mode Function*:

$$IMF(x) = \frac{1}{2} \left( \hat{f}(x) + \check{f}(x) \right)$$

4. Iterate this process (that is called the *sifting process*) on the residual, *i.e.*,

$$r(x) = f(x) - IMF(x)$$

71 until a selected tolerance criterion is respected.

72 Thus, the original signal is decomposed as:

$$73 \quad (1.1) \quad f(x) = \sum_{k=1}^n IMF_k(x) + r(x)$$

74 where  $IMF_k$  is the  $k$ -th intrinsic mode function and  $r$  is the last residual. The EMD can be  
 75 efficiently applied to 1D-signals. However the selection of interpolation method for the second  
 76 step gives a wide variety of possibilities, from the original formulation using cubic splines [24],  
 77 passing by sparse filtering [23], filtering from wavelet based decomposition [15] and partial  
 78 differential equation based formulations [10].

79 The EMD method can be justified only under certain very restrictive assumptions that  
 80 are seldom satisfied by practical data. The EMD method is also known to be very sensitive  
 81 to noisy data. Recently, a compendium of practical advice for EMD in real life examples  
 82 has been presented in [51]. Some works extend EMD to 2D [12, 50, 11] and 3D images [19].  
 83 However, the main limitations of EMD for both 2D and 3D are both the choice of maxima  
 84 and minima detector, and the choice of the interpolation algorithm.

85 An alternative characterisation of the EMD computation was introduced by Diop *et al.* in  
 86 [12, 13] according to the definition of *local mean*, *i.e.*, the sifting process is fully determined  
 87 by the sequence  $(h_n)_{n \in \mathbb{N}}$  defined by :

$$88 \quad (1.2) \quad \begin{cases} h_{n+1} = h_n - \Phi(h_n) = (\text{Id} - \Phi) h_n \\ h_0 = f \end{cases}$$

89 where  $\Phi(h_n) = \frac{\hat{h}_n + \check{h}_n}{2}$ , and  $\hat{h}_n$  (resp.  $\check{h}_n$ ) denotes a continuous interpolation of the maxima  
 90 (resp. minima) of  $h_n$ .

91 In the following subsection, we formulated an EMD by means of dilation and erosion  
 92 operators.

93 **1.1.2. Dilation/Erosion.** We study here functions  $f : E \rightarrow \overline{\mathbb{R}}$ , where  $\overline{\mathbb{R}}$  it allowed to be  
 94 *extended-real-valued*, *i.e.*, to take values in  $\overline{\mathbb{R}} = [-\infty, \infty]$ . Accordingly, the set of all such  
 95 functions is denoted by  $\mathcal{F}(E, \overline{\mathbb{R}})$ . We will use the two basic morphological operators *dilation*  
 96 and *erosion*, which correspond respectively to the convolution in the  $(\max, +)$  algebra and its  
 97 dual.

98 **Definition 1.1.** *In mathematical morphology [48], the dilation (sup-convolution)  $\delta_{SE}(f)$  of*  
 99  *$f$  is given by:*

$$100 \quad (1.3) \quad \delta_{SE}(f)(x) := \sup_{y \in E} \{f(y) + SE(x - y)\} = \sup_{w \in E} \{f(x - w) + SE(w)\}$$

101 where  $SE \in \mathcal{F}(E, \overline{\mathbb{R}})$  is the (additive) structuring function which determines the effect of the  
 102 operator. Here the *inf-addition rule*  $\infty - \infty = \infty$  is to be used in case of conflicting infinities.  
 103  $\sup f$  and  $\inf f$  refer to the supremum (least upper bound) and infimum (greatest lower bound)  
 104 of  $f$ . In the discrete case where the function is a finite set of points,  $\max$  and  $\min$  are used.

105 The erosion [48]  $\varepsilon_{SE}(f)$ , known as *inf-convolution* in convex analysis [36], is the adjoint  
 106 operator to the dilation (1.3), and it is defined as

$$107 \quad (1.4) \quad \varepsilon_{SE}(f)(x) := -\delta_{\check{SE}}(-f)(x) = \inf_{y \in E} \{f(y) - SE(y - x)\} = \inf_{w \in E} \{f(w - x) - SE(w)\}$$

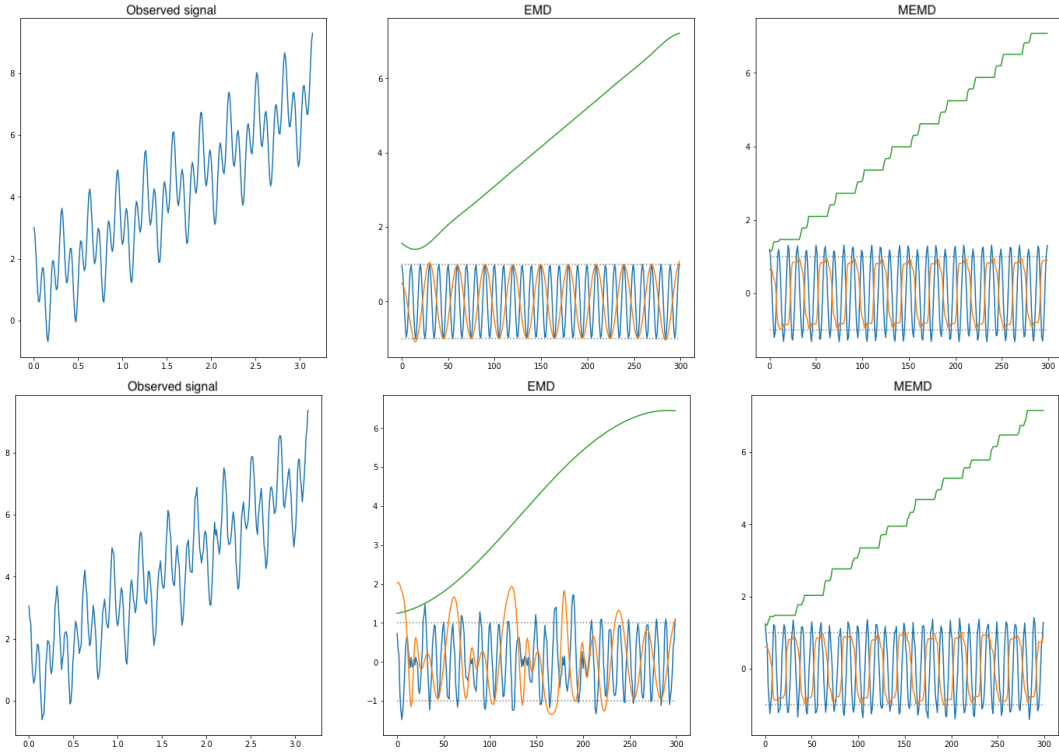


**Figure 1.** First Row: Noise-free example a)  $f(x) = 2x+1+\cos(20x)+\cos(60x)$ , b) Classical EMD c) MEMD with flat structuring functions. Second Row: Noisy example a)  $f(x) = 2x + 1 + \cos(20x) + \cos(60x) + N(0, \frac{1}{8})$ , b) Classical EMD c) MEMD with flat structuring functions.

108 where the transposed structuring function is  $\check{S}E(x) = SE(-x)$ .

109 *Remark 1.2.*  $\forall f, g \in \mathcal{F}(E, \overline{\mathbb{R}})$

- 110 1. The operators (1.3) and (1.4) are translation invariant.
- 111 2. (1.3) and (1.4) correspond to one another through the duality relation  $\delta_{SE}(f)(x) \leq$   
112  $g(x) \iff f(x) \leq \varepsilon_{SE}(g)(x)$ , called *adjunction* [16].
- 113 3. An operator  $\xi$  is called *increasing* if  $f(x) \geq g(x) \Rightarrow \xi(f)(x) \geq \xi(g)(x) \forall x$ . The dilation  
114 (1.3) and erosion (1.4) are increasing for all SE.
- 115 4. An operator  $\xi$  is called *extensive* (resp. *antiextensive*) if  $\xi(f)(x) \geq f(x)$  (resp.  
116  $\xi(f)(x) \leq f(x)$ ),  $\forall x$ . The dilation (1.3) (resp. erosion (1.4)) is extensive (resp. antiex-  
117 tensive) if and only if  $SE(0) \geq 0$ , *i.e.*, the structuring function evaluated at the origin  
118 is non-negative.
- 119 5.  $\varepsilon_{SE}(f)(x) \leq f(x) \leq \delta_{SE}(f)(x)$  if and only if  $SE(0) \geq 0$ .
- 120 6.  $\delta_{SE}$  (resp.  $\varepsilon_{SE}$ ) does not introduce any local maxima (resp. local minima) if  $SE \leq 0$   
121 and  $SE(0) = 0$ . In this case, we say that SE is *centered*.

122 *Proof.* (1) and (2) are classical results from [48]. As explained in [21] and [31], the *adjunc-*  
123 *tion* is related to a well-known concept in group and lattice theory, the *Galois connection*. (3)  
124 and (6) are easy to prove directly from the definition of the operators. It has been also proved

125 in the original paper of inf-convolution (Proposition 6.d) in [36]. (4)  $\forall f, \delta_{SE}(x) \geq f(x) \Rightarrow$   
 126  $\forall f, \sup (f(x-w) + SE(w) - f(x)) (x) \geq 0 \Rightarrow SE(0) \geq 0$ . Now,  $\sup f(x-w) + SE(w) \geq$   
 127  $f(x) + SE(0)$ , if  $SE(0) \geq 0 \Rightarrow \sup f(x-w) + SE(w) \geq f(x)$ . From (3) and (4) is easy to prove  
 128 (5). ■

129 The most commonly studied framework for dilation/erosion of functions is based on *flat struc-*  
 130 *turing functions*, where structuring elements are viewed as *shapes*. More precisely, given the  
 131 structuring element  $B \subseteq E$ , its associated structuring function is

$$132 \quad (1.5) \quad B(y) = \begin{cases} 0 & \text{if } y \in B \\ -\infty & \text{if } y \in B^c \end{cases}$$

133 Hence, the flat dilation  $\delta_B(f)$  and flat erosion  $\varepsilon_B(f)$  can be computed respectively by the  
 134 moving local maxima and minima filters. The shape of  $B$  is often a disk of radius  $\lambda$ , denoted  
 135 by  $B_\lambda$ .

$$136 \quad (1.6) \quad B_\lambda(w) = \begin{cases} 0 & \text{if } \|w\| \leq \lambda \\ -\infty & \text{if } \|w\| > \lambda \end{cases}$$

137 A Morphological Empirical Mode Decomposition (MEMD) where the pair  $(\hat{h}, \check{h})$  correspond  
 138 to  $(\varepsilon_{B_\lambda}, \delta_{B_\lambda})$  has been proposed in [13].

139 **Definition 1.3.** *The Flat Morphological Empirical Mode [13] is defined as*

$$140 \quad (1.7) \quad \Phi_{\varepsilon, \delta, B_\lambda}(f)(x) := \frac{\delta_{B_\lambda}(f)(x) + \varepsilon_{B_\lambda}(f)(x)}{2}$$

141 The operator (1.7) was proposed to generate an EMD based on solving a morphological PDE  
 142 [13]. As a manner of example, EMD and MEMD are shown for a mono-component signal in  
 143 the first row of Figure 1. In the second row of Figure 1, we illustrated how the addition of  
 144 noisy perturbed more the results of classical EMD than the proposed morphological one.

145 **Remark 1.4.** Note that using (1.7) twice, the first residual (1.2) is  $2(f - \Phi_\lambda(f)) = (f -$   
 146  $\delta_{B_\lambda}(f)) + (f - \varepsilon_{B_\lambda}(f)) = 2f - \delta_{B_\lambda}(f) - \varepsilon_{B_\lambda}(f)$ . This expression, up to a minus sign, cor-  
 147 responds just to the so-called *morphological Laplace operator* [54], and therefore provides an  
 148 interpretation of the EMD as an iterated second-order derivative decomposition of the function  
 149  $f$ .

150 **1.2. Our proposal.** The main motivation of this paper is to define EMD learnable in the  
 151 sense of neural networks approaches. Note that last property in Remark 1.2 together with  
 152 the extensivity/antiextensivity (*i.e.*, upper/lower envelopes) imply that the pair of operators  
 153  $(\varepsilon_{SE}, \delta_{SE})$  are candidate functions for  $(\hat{h}, \check{h})$  in (1.2). Accordingly, we proposed a simple  
 154 generalization by considering non-flat structuring functions.

155 **Definition 1.5.** *The Morphological Empirical Mode (MEM) is defined as*

$$156 \quad (1.8) \quad \Phi_{\varepsilon, \delta, SE}(f) = \frac{\delta_{SE}(f)(x) + \varepsilon_{SE}(f)(x)}{2}$$

157 This operator can be formulated in any dimension (from 1D to nD signals) and avoid using  
 158 an interpolation method which is the bottleneck of the original definition of EMD.

159 **1.3. Contributions of the paper.** In what follows we study,

- 160 • A formulation of EMD based on pairs of morphological operators in a general case.
- 161 • The proposition of a parametric morphological empirical mode whose sifting process
- 162 is invariant to additive intensity shifts.
- 163 • A approach to learn the structuring functions of a morphological operator in a deep
- 164 learning framework.
- 165 • A convex sum of envelopes instead of mean points to learn morphological EMD.
- 166 • A number of numerical experiments for hyperspectral signal classification to illustrate
- 167 the relevance of our proposal.

168 **1.4. Organization of the paper.** The rest of the paper is organised as follows. In [sec-](#)  
 169 [tion 2](#), we review the general definition of Empirical Mode Decomposition approach to decom-  
 170 pose signals and we introduce how morphological extensive/antiextensive filters are naturally  
 171 adapted to implement a MEMD computation. We consider different possibilities in the choice  
 172 of structuring functions and the pair of lower and upper envelopes. Additionally, an  $\alpha$ -MEM  
 173 is proposed as a generalization of the mean of envelopes. [Section 3](#) is devoted to the imple-  
 174 mentation of morphological EMD operators as layers in a neural network pipeline. [Section 4](#)  
 175 presents the experimental results of hyperspectral image classification using DCNNs which  
 176 integrate morphological EMD layers. Conclusions and perspectives are discussed in [section 5](#).

177 **2. Morphological Empirical Mode and its variants.** In this section, three kinds of gen-  
 178 eralization will be explored: a) different types of structuring functions, b) different pairs of  
 179 functions to compute the lower and upper envelopes, and c) a convex sum of lower and upper  
 180 envelopes.

181 **2.1. Varying the structuring function.** In this subsection, firstly we will study a paramet-  
 182 ric family of symmetric quadratic shape structuring functions. Secondly, similarly to classical  
 183 CNNs, the structuring function plays a similar role to the kernel in standard convolution.  
 184 Accordingly a structuring function without any parametric constraint is also considered.

185 **2.1.1. Quadratic MEM.** From the theory of morphological scale-spaces, the most useful  
 186 nonflat structuring functions are those which depend on a scale parameter [[22](#), [47](#)]. The only  
 187 separable and rotationally invariant structuring functions is the called *quadratic structuring*  
 188 *function*[[52](#)]:

$$189 \quad (2.1) \quad q_\lambda(z) = -\frac{\|z\|^2}{2\lambda},$$

190 such that the corresponding dilation and erosion are equal to the Lax–Oleinik operators or  
 191 viscosity solutions of the standard Hamilton–Jacobi PDE, also known as morphological PDE:  
 192  $u_t(t, x) \mp \|u_x(t, x)\|^2 = 0$ ,  $(t, x) \in (0, +\infty) \times E$ ;  $u(0, x) = f(x)$ ,  $x \in E$ . It plays also a canonical  
 193 role in the definition of dilation and erosion on Riemannian manifolds [[2](#)] and their behaviour  
 194 with respect to the maxima/minima is well understood [[26](#)]. The morphological PDE was  
 195 proposed and analyzed using 2D boundary propagation in [[53](#)] and further analyzed using the  
 196 morphological slope transform in [[20](#)].

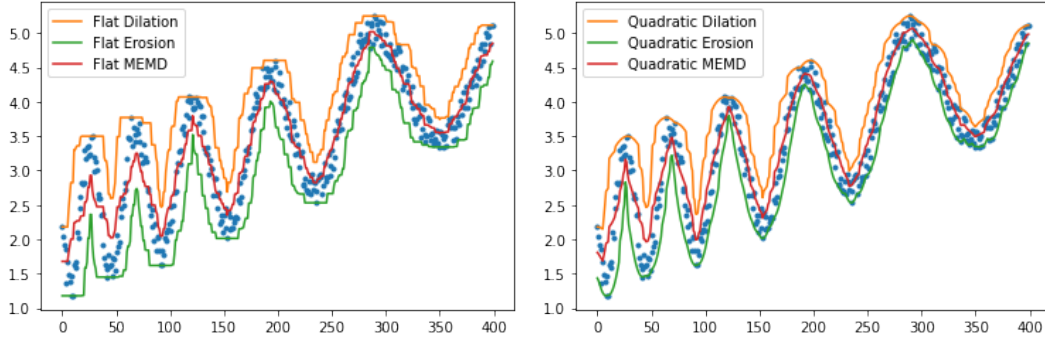


**Figure 2.** The blue points corresponds to the observed signal, a) Flat dilation/erosion based Morphological Empirical Mode (1.7) with a disk of  $\lambda = 5$ , b) Quadratic dilation/erosion based Morphological Empirical Mode (2.3) with  $\lambda = 3$ .

197 *Remark 2.1.* The erosion by a quadratic structuring function with parameter  $\lambda$  is defined  
 198 by  
 (2.2)

$$199 \quad \varepsilon_{q_\lambda}(f)(x) := \inf_{y \in E} \{f(y) - q_\lambda(y - x)\} = \inf_{z \in E} \{f(z - x) - q_\lambda(z)\} = \inf_{z \in E} \left\{ f(z - x) + \frac{\|z\|^2}{2\lambda} \right\}.$$

200 The erosion of a function  $f$  by a quadratic structuring function with parameter  $\lambda$  is  
 201 known as the *Moreau envelope* or *Moreau-Yosida approximation* [36, 44, 41], which offers  
 202 many benefits specially for optimization purposes [35]. Additionally, (2.2) induces an additive  
 203 scale-space [20, 25], i.e.,  $\varepsilon_{q_{\lambda_1}}(\varepsilon_{q_{\lambda_2}}(f)) = \varepsilon_{q_{\lambda_1 + \lambda_2}}(f)$ .

204 *Definition 2.2.* The quadratic morphological empirical mode (QMEM) is defined as a MEM  
 205 where the pair  $(\hat{h}, \check{h})$  corresponds to erosion/dilation with a quadratic structuring functions,

$$206 \quad (2.3) \quad \Phi_{\varepsilon, \delta, q_\lambda}(f) = \frac{\varepsilon_{q_\lambda}(f) + \delta_{q_\lambda}(f)}{2}.$$

207 An example of (2.3) for a 1D signal with noise is shown in Figure 2.

208 **2.1.2. Nonflat Morphological MEM.** The most general case of *nonflat structuring func-*  
 209 *tion* involves different additive weights  $W_y(x)$  at each position  $x$  of the local neighborhood  $B$   
 210 centered at pixel  $y$ , i.e., a nonflat structuring function  $SE_W$  of support shape  $B$  at  $y$  is defined  
 211 as

$$212 \quad (2.4) \quad SE_{W_y}(x) = \begin{cases} W_y(x) & \text{if } x \in B(y) \\ -\infty & \text{otherwise} \end{cases}$$

213 The case (2.4) includes flat, nonflat, either local or nonlocal structuring functions [55]. In the  
 214 translation invariant case, the weighting function  $W_y(x)$  is equal for all  $y \in E$ .

215 **2.2. Varying the Envelope.** We have explored above several possible structuring functions  
 216 that produce multiple pairs of  $(\varepsilon_{SE}, \delta_{SE})$  as basic ingredient for the Morphological Empirical  
 217 Mode (1.8). At this point, we can consider the use of the composition of erosion and dilation  
 218 to obtain other upper/lower envelopes, typically of the form  $(\delta_{SE} \circ \varepsilon_{SE}, \varepsilon_{SE} \circ \delta_{SE})$ .



219 **2.2.1. Opening/Closing MEM.** The theory of morphological filtering is based on the  
 220 opening  $\gamma_{SE}(f)(x)$  and closing  $\varphi_{SE}(f)(x)$  operators, obtained respectively by the composi-  
 221 tion product of erosion-dilation and dilation-erosion, *i.e.*,  $\gamma_{SE}(f)(x) = \delta_{SE}(\varepsilon_{SE}(f))(x)$  and  
 222  $\varphi_{SE}(f)(x) = \varepsilon_{SE}(\delta_{SE}(f))(x)$ . Opening (resp. closing) is increasing, idempotent and anti-  
 223 extensive (resp. extensive), independently of the properties of the structuring function. The  
 224 opening can be seen as the supremum of the invariants parts of  $f$  under-swept by SE and it  
 225 can be again rewritten as a maximal lower envelope of structuring functions (resp. minimal  
 226 upper envelope of negative symmetric structuring functions). We highlight that the *quadratic*  
 227 *envelope* also called as *proximal hull* [7] is an opening with a quadratic structuring function,  
 228 *i.e.*, a quadratic erosion followed by a quadratic dilation.

229 **Definition 2.3.** *The opening/closing morphological empirical mode (OCMEM) is defined as*  
 230 *a MEM where the pair  $(\hat{h}, \hat{h})$  corresponds to  $(\gamma_{SE}, \varphi_{SE})$ , *i.e.*,*

$$231 \quad (2.5) \quad \Phi_{\gamma, \varphi, SE}(f) = \frac{\gamma_{SE}(f) + \varphi_{SE}(f)}{2}.$$

232 For the case of flat disks  $B_\lambda$ , the operator (2.5) was called a morphological locally monotonic  
 233 (LOMO) filter in [5]. A signal is monotonic over an interval if it is either non-increasing or  
 234 non-decreasing over that interval. A 1-D signal is *locally monotonic* of degree  $n$  (LOMO- $n$ )  
 235 if and only if the signal is monotonic within every interval of length  $n$ . In the general case, a  
 236 LOMO filter of  $f$  is defined as the fixed point of iterating  $\Phi_{\gamma, \varphi, B_\lambda}(f)$ , which is simultaneously  
 237 idempotent to both the opening and closing by a flat disk as structuring function. Two  
 238 examples of (2.5) for both flat and quadratic structuring function for the 1D signal with noise  
 239 are shown in Figure 3.

240 **2.2.2. Lasry–Lions MEM.** Besides their feature extraction properties, morphological di-  
 241 lation and erosion using quadratic structuring functions are a powerful tool for Lipschitz  
 242 regularization. For the nonconvex case, the Lasry–Lions double envelope is defined as the  
 243 composition of two different Moreau envelopes, or using the morphological vocabulary, the  
 244 composition of an erosion followed by a dilation with quadratic structuring functions. For all  
 245  $0 < c < 1$  and  $0 < \lambda$ , the so-called Lasry–Lions regularizers [28] are defined as

$$246 \quad \gamma_\lambda^c(f)(x) := \delta_{q_{c\lambda}}(\varepsilon_{q_\lambda}(f))(x),$$

$$247 \quad \varphi_\lambda^c(f)(x) := \varepsilon_{q_{c\lambda}}(\delta_{q_\lambda}(f))(x),$$

248 such that if  $f$  is bounded, the functions  $\gamma_\lambda^c$  and  $\varphi_\lambda^c$  are bounded and one has the ordering  
 249 properties for the following envelopes:

- 250 • if  $\lambda_1 \geq \lambda_2 > 0$ , for any  $0 < c < 1$  then

$$251 \quad \gamma_{\lambda_1}^c(f)(x) \leq \gamma_{\lambda_2}^c(f)(x) \leq f \leq \varphi_{\lambda_2}^c(f)(x) \leq \varphi_{\lambda_1}^c(f)(x);$$

- 252 • if  $0 < c_2 < c_1 < 1$ , for any  $\lambda > 0$  then

$$253 \quad \gamma_\lambda^{c_2}(f)(x) \leq \gamma_\lambda^{c_1}(f)(x) \leq f \leq \varphi_\lambda^{c_1}(f)(x) \leq \varphi_\lambda^{c_2}(f)(x).$$

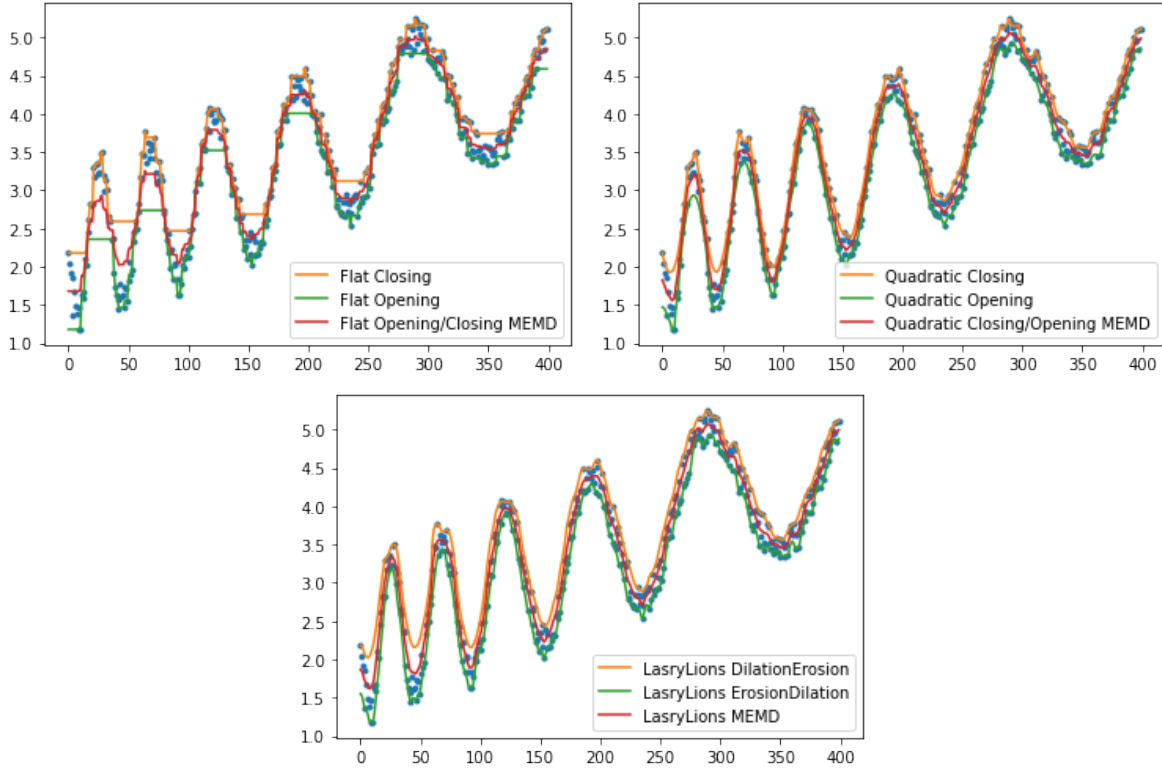


**Figure 3.** a) Flat OCMEM with a disk of  $\lambda = 5$ , b) Quadratic OCMEM with  $\lambda = 3$  and c) Lasry-Lions MEM with  $\lambda = 3$  and  $c = .9$

254 For any bounded function  $f$ , Lasry–Lions regularizers provide a function with a Lipschitz  
 255 continuous gradient, *i.e.*,

$$256 \quad |\nabla \gamma_\lambda^c(f)(x) - \nabla \gamma_\lambda^c(f)(y)| \leq M_{\lambda,c} \|x - y\|, \quad |\nabla \varphi_\lambda^c(f)(x) - \nabla \varphi_\lambda^c(f)(y)| \leq M_{\lambda,c} \|x - y\|.$$

257 where the Lipschitz constant is  $M_{\lambda,c} = \max((c\lambda)^{-1}, ((1-c)\lambda)^{-1})$ . If  $f$  is bounded and  
 258 Lipschitz continuous, one has

$$259 \quad \text{Lip}(\gamma_\lambda^c(f)) \leq \text{Lip}(f) \text{ and } \text{Lip}(\varphi_\lambda^c(f)) \leq \text{Lip}(f),$$

260 with

$$261 \quad \text{Lip}(g) = \sup \left\{ \frac{|g(x) - g(y)|}{\|x - y\|}; x, y \in \mathbb{R}^n, x \neq y \right\}.$$

262 For more details on the properties of Lasry–Lions regularizers in the context of mathe-  
 263 matical morphology, see [1].

264 *Remark 2.4.* The following statements are interesting about the composition of quadratic  
 265 morphological operators [44, 9]. Let  $0 < \mu < \lambda$ ,

- 266 1.  $\varepsilon_{q_\lambda}(\gamma_{q_\lambda}(f)) = \varepsilon_{q_\lambda}(f)$ ;  
 267 2.  $\gamma_{q_\mu}(\varepsilon_{q_{\lambda-\mu}}(f)) = \varepsilon_{q_{\lambda-\mu}}(\gamma_{q_\lambda}(f))$ ;  
 268 3.  $\gamma_{q_{\lambda-c\lambda}}\varphi_\lambda^c(f) = \varphi_\lambda^c(f)$ .

269 **Definition 2.5.** *The Lasry-Lions morphological empirical mode (LLMEM) is defined as a*  
 270 *MEM where the pair  $(\hat{h}, \check{h})$  corresponds to  $(\gamma_\lambda^c, \varphi_\lambda^c)$ , i.e.,*

$$271 \quad (2.6) \quad \Phi_{\gamma, \varphi, c, \lambda}(f) := \frac{\gamma_\lambda^c(f) + \varphi_\lambda^c(f)}{2}.$$

272 An example of (2.6) for a 1D signal is shown in Figure 3(c).

273 **2.3. Parametric family of morphological empirical mode operator.** The choices of the  
 274 structuring function and the class of lower and upper envelopes give extra possibilities for the  
 275 formulation of an EMD approach. Besides, a third degree of freedom is considered now by  
 276 including a parameter to weight the contribution of the two envelopes. We have been inspired  
 277 by the recent work on proximal average [9] to propose a convex generalization of MEMs.

278 **Definition 2.6.** *Let  $\alpha$  be a real value with  $0 \leq \alpha \leq 1$ , the  $\alpha$ -Morphological Empirical Mode*  
 279 *based on the pair  $(\hat{h}, \check{h})$  is defined as:*

$$280 \quad (2.7) \quad \Phi_{\hat{h}, \check{h}}^\alpha(f) = \alpha \hat{h}(f) + (1 - \alpha) \check{h}(f).$$

281 **Definition 2.7.** *Let  $T_g : \mathcal{F}(E, \overline{\mathbb{R}}) \mapsto \mathcal{F}(E, \overline{\mathbb{R}})$  be a set of transformations on the space  $E$  for*  
 282 *the abstract group  $g \in G$ . We say a function  $\phi$  is invariant to  $g$  if for all transformations  $T_g$ ,*  
 283 *and for all  $f \in \mathcal{F}(E, \overline{\mathbb{R}})$  one has*

$$284 \quad (2.8) \quad \phi(T_g(f)) = \phi(f)$$

285 *This says that the feature extracted by  $\phi$  does not change as the transformation is applied to*  
 286 *the input.*

287 In this context, an important fact to consider are the invariances of the operator (2.7).

288 **Remark 2.8.** For any SE,  $\forall 0 \leq \alpha \leq 1$ , and all the pairs  $(\check{h}, \hat{h})$  previously considered, the  
 289 operator (2.7) is increasing, invariant to translation, and the sifting process  $f - \Phi_{\hat{h}, \check{h}}^\alpha(f)$  is  
 290 invariant to additive intensity shifts, i.e.,  $\forall c \in \mathbb{R}$  and  $\forall f \in \mathcal{F}(E, \overline{\mathbb{R}})$ ,

$$291 \quad (f(x) + c) - \Phi_{\hat{h}, \check{h}}^\alpha(f(x) + c) = f(x) - \Phi_{\hat{h}, \check{h}}^\alpha(f(x)).$$

292 **3. Learnable Morphological Empirical Mode Decomposition.** One of the main advan-  
 293 tages of EMD is that it can be considered as a parameter-free decomposition [51] and, for  
 294 this reason, the inclusion of the structuring function and the parameter  $\alpha$  can be seen as  
 295 inconvenient. However, in the following, we consider EMD in the context of learning from  
 296 data [30], where one would be interested in using EMD decomposition as a preprocessing of  
 297 an input signal before using a machine learning or deep learning methods [43, 3, 27].

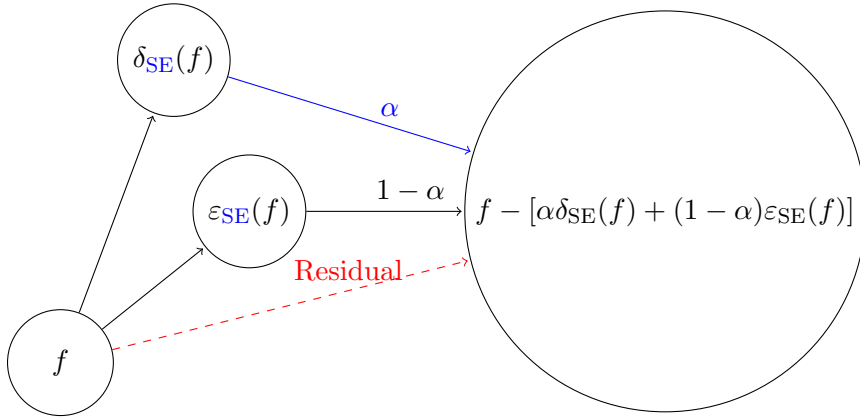


**Figure 4.** The Morphological Empirical Mode layer with input  $f$  corresponds to a residual layer [18] where the processing block is the average between upper and lower envelopes  $(\hat{h}, \hat{h})$ , in this case the pair  $(\varepsilon, \delta)$  is used as example. In the experimental section that is used as a preprocessing layer for high-dimensional supervised classification problems. The parameters of the layer are highlighted in blue.

298 **3.1. Neural network-based learning of parameters.** The simplest form of a neural network  
 299 is the called *multilayer architecture*, which is a stack by composition of modules, each  
 300 module implements a function  $X_n = F_n(\theta_n, X_{n-1})$ , where  $X_n$  is a vector representing the  
 301 output of module,  $\theta_n$  is the vector of learnable parameters in the module, and  $X_{n-1}$  is the  
 302 module input vector (as well as the output of the previous module). The input of the first  
 303 module  $X_0$  is an input pattern  $Z_0$ , the output of the whole system is the one of the last module  
 304 which denoted  $Z_l$ , where  $l$  is the *number of layers*. In *gradient-based learning methods*,  
 305 given a cost function  $\mathcal{L}^p(\cdot, \cdot)$  measuring the discrepancy between the output of the system  
 306  $Z_l^p$  and  $D^p$  the “correct” or desired output for the  $p$ -th input pattern. One is interested on  
 307 minimizing the average discrepancy over a set of input/output pairs called the *training set*,  
 308  $\{(Z_0^0, D^0), (Z_0^1, D^1), \dots, (Z_0^n, D^n)\}$ . The network is initialized with randomly chosen weights  
 309  $\theta^0$ . The gradient of the error function with respect to each parameter is computed and gradient  
 310 descent is used to update the weights in each layer, *i.e.*, for the  $i$ -th iteration,  $\theta^{i+1} = \theta^i - \eta \frac{\partial \mathcal{L}(\theta)}{\partial \theta^i}$   
 311 where  $\eta$  is a learning rate, and the computation of  $\frac{\partial \mathcal{L}(\theta)}{\partial \theta^i}$ , is performed by *backpropagation algorithm*  
 312 through the layers [45]. Additionally, for structured data as images, *convolutional*  
 313 *neural networks* (CNN) are nowadays the recommended solution. In CNNs, the same operator  
 314 is computed in each pixel of the image. This mechanism is called *weight sharing*, and it has  
 315 several advantages such as it can reduce the model complexity and make the network easier  
 316 to train [39]. Including any new layer, like EMD, requires therefore the computation of the  
 317 corresponding gradient of the layer with respect to the parameters to be learnt.

318 **3.2. Derivatives of Morphological EMD in discrete domains.**

319 **3.2.1. Derivative of dilation and erosion.** Our approach involves dilation and erosion  
 320 operators as defined in (1.3) and (1.4). However, in the discrete domain as it is the case  
 321 of  $nD$  images, the sup operator is computed via max. Consequently, for dilation operator  
 322 (1.3), is computed by  $\delta_\lambda(x) = \max_w \{f(x-w) + SE_\lambda(w)\}$ . To understand how to compute  
 323 the derivative of  $\delta_\lambda(x)$  with respect  $\lambda$ , we rewrite  $\delta_\lambda(x) = \max_{w \in SE_\lambda} u(w)$ . The max operator  
 324 has no gradient with respect to non-maximum values, since changing them slightly does not

325 affect the output. In general for rank operators, their derivative is zero in every coordinate,  
 326 except for that of the value attending the desired rank [42, 37]. Accordingly, the derivative  
 327 with respect of a parameter in the additive structuring function is given by

$$328 \quad (3.1) \quad \frac{\partial \delta_\lambda(x)}{\partial \lambda} = \frac{\partial \delta_\lambda(x)}{\partial u(w)} \frac{\partial u(w)}{\partial \lambda} = \begin{cases} \frac{\partial \text{SE}_\lambda(w)}{\partial \lambda} & \text{if } w \in \arg \max_x \delta_\lambda(x) \\ 0 & \text{otherwise} \end{cases}$$

329 where the operator  $\arg \max_x f(x) := \{x \mid \forall y : f(y) \leq f(x)\}$ . In other words,  $\arg \max$  is  
 330 the set of points  $x$ , for which  $f(x)$  attains the largest value of the function. Note that we  
 331 do not regard maximum as being attained at any  $x$  when  $f(x) = \infty$ , nor do we regard the  
 332 minimum as being attained at any  $x$  when  $f(x) = -\infty$ . Similarly for the erosion,  $\varepsilon_\lambda(x) =$   
 333  $\min_w [f(x+w) - \text{SE}_\lambda(w)] = \min_{w \in \text{SE}_\lambda} u(w)$

$$334 \quad (3.2) \quad \frac{\partial \varepsilon_\lambda(x)}{\partial \lambda} = \frac{\partial \varepsilon_\lambda(x)}{\partial u(w)} \frac{\partial u(w)}{\partial \lambda} = \begin{cases} -\frac{\partial \text{SE}_\lambda(w)}{\partial \lambda} & \text{if } w \in \arg \min_x \varepsilon_\lambda(x) \\ 0 & \text{otherwise} \end{cases}$$

335 there is only gradient with respect to minimum values.

336 As a manner of example, for the dilation by quadratic structuring element (2.1), one has

$$337 \quad \frac{\partial q_\lambda(z)}{\partial \lambda} = (2\lambda^2)^{-1} \|z\|^2 \implies \frac{\partial \delta_\lambda(x)}{\partial \lambda} = \begin{cases} \frac{\|w\|^2}{2\lambda^2} & \text{if } w \in \arg \max_x \delta_\lambda(x) \\ 0 & \text{otherwise} \end{cases}$$

338 Therefore, for Quadratic EMD (2.3) the derivative with respect of  $\lambda$ ,

$$339 \quad \frac{\partial \Phi_\lambda(x)}{\partial \lambda} = \frac{\|w_\delta\|^2 - \|w_\varepsilon\|^2}{4\lambda^2},$$

340 where  $w_\delta \in \arg \max_x \delta_\lambda(x)$  and  $w_\varepsilon \in \arg \min_x \varepsilon_\lambda(x)$ . Thus, the evolution of the parameter  
 341  $\lambda$  depends on the difference of the norm to the value where the morphological operator at-  
 342 tends their value, normalised by the square of the current value of  $\lambda$ . Curiously the nonflat  
 343 translation invariant MEM (2.4) has a derivative that does not depend on the scale of the  
 344 parameters, *i.e.*, for  $\text{SE}_W = [w_0, \dots, w_k]$ ,

$$345 \quad (3.3) \quad \frac{\partial \Phi_{\text{SE}_W}(x)}{\partial w_i} = \begin{cases} 1/2 & \text{if } w_i \in \arg \max_x \delta_{\text{SE}_W}(x) \\ -1/2 & \text{if } w_i \in \arg \min_x \varepsilon_{\text{SE}_W}(x) \\ 0 & \text{otherwise} \end{cases}$$

346 Finally, the derivative for composition operators, as opening or closing, can be easily compute  
 347 by the chain rule.

348 **3.3. Implementation.** Different methods for learning morphological operators in neural  
 349 networks have been proposed in the literature:

- 350 1. Replace maximum and minimum operator by smooth differentiable approximations,  
 351 making possible the use of conventional gradient descent learning approach via back-  
 352 propagation, for instance using an approximation by counter-harmonic mean [33] or  
 353 other generalizations [29].

354 2. Morphological operations can be computed by combinations of depthwise and point-  
 355 wise convolution with depthwise pooling [38] allowing the use of classical optimization  
 356 procedures.

357 3. Use original definition of morphological operator, and in the backpropagation step  
 358 follows the approach used in max-pooling layers [6, 14, 34].

359 We follow the last approach. That means that the gradient in (3.1) and (3.2) will have val-  
 360 ues different from zero *only* for the first element equal to the arg max or argmin instead  
 361 of the complete equivalence class. This is the implementation used in deep learning mod-  
 362 ules based on Tensorflow or Pytorch. An implementation of our approach is available in  
 363 <http://www.cmm.mines-paristech.fr/~velasco/morpholayers/>

364 **3.3.1. Example of learning parameters in morphological operators.** We present a dummy ■  
 365 example of supervised classification in two classes for 1D signals of dimension  $p$ . Both classes  
 366 have been generated by the function  $f(x) = \sin(\frac{2\pi}{c}(x + \epsilon))$ , for  $x = 0, \dots, 10$ , with spatial  
 367 step of 0.02 and where  $\epsilon$  is a random realisation of a normalized Gaussian distribution. For  
 368 the first class, we have used a period  $c = 2$  and for the second class a period  $c = 1.75$ . Some  
 369 examples are illustrated in Figure 5(a). We explore the training process by using a simple  
 370 architecture:  $\hat{z} := model(x) = \frac{1}{1 + \exp(-\frac{1}{p} \sum_{i=1}^p \delta_\lambda(x_i))}$ , *i.e.*, a morphological dilation followed by  
 371 a global average pooling with a sigmoid activation function, also called the logistic function.  
 372 Now, we want to show the computation of the partial derivative with respect to a given loss  
 373 function. As a manner of example, we use the mean squared error as a loss function, *i.e.*,  
 374  $loss(z, \hat{z}) = (z - \hat{z})^2$ .

375 One can compute the gradient  $\frac{\partial loss(z, \hat{z})}{\partial \lambda}$  by using the chain rule of derivative

$$376 \quad \frac{\partial loss(z, \hat{z})}{\partial \lambda} = \frac{\partial loss(z, \hat{z})}{\partial \hat{z}} \frac{\partial \hat{z}}{\partial \sigma} \frac{\partial \sigma}{\partial \sum \delta_\lambda / p} \frac{\partial \sum \delta_\lambda / p}{\partial \lambda},$$

377 where  $\sigma(x) := \frac{1}{1 + \exp(-x)}$  is the sigmoid function. Remember that the derivative of the sigmoid  
 378 function is  $\sigma(x)\sigma(1-x)$ . By defining  $m = \sum_{i=1}^p \delta_\lambda(x_i) / p$ , the mean value of the dilation, which  
 379 is used as decision function, the derivative of the parameter of the dilation with respect to the  
 380 loss function can be written by

$$381 \quad \frac{\partial loss(z, \hat{z})}{\partial \lambda} = \frac{(2m)(m(1-m))}{p} \sum_{i=1}^p \frac{\partial \delta_\lambda(x)}{\partial \lambda}.$$

382 The first term is computed in the forward pass and it is the same for every parameter. We  
 383 decided to train a nonflat structuring function, so from (3.3), one can interpret the second  
 384 term as a counts the number of number of times that the spatial position in the structuring  
 385 function attains the maximal value, which is illustrated in Figure 5(c) for the last epoch of the  
 386 training. Additionally, the evolution of structuring function weights is given in Figure 5(d).  
 387 As a manner of example, two signals and its corresponding learned dilation are shown for the  
 388 initialization (as a flat structuring function) in Figure 5(e) and after convergence in Figure 5(f).  
 389 Finally, the decision function (mean value of the learned dilation) is shown for all the training  
 390 examples at initialisation Figure 5(g) and after convergence Figure 5(h). We highlight that  
 391 the learned structuring function seems to be an asymmetric quadratic with an additive bias.

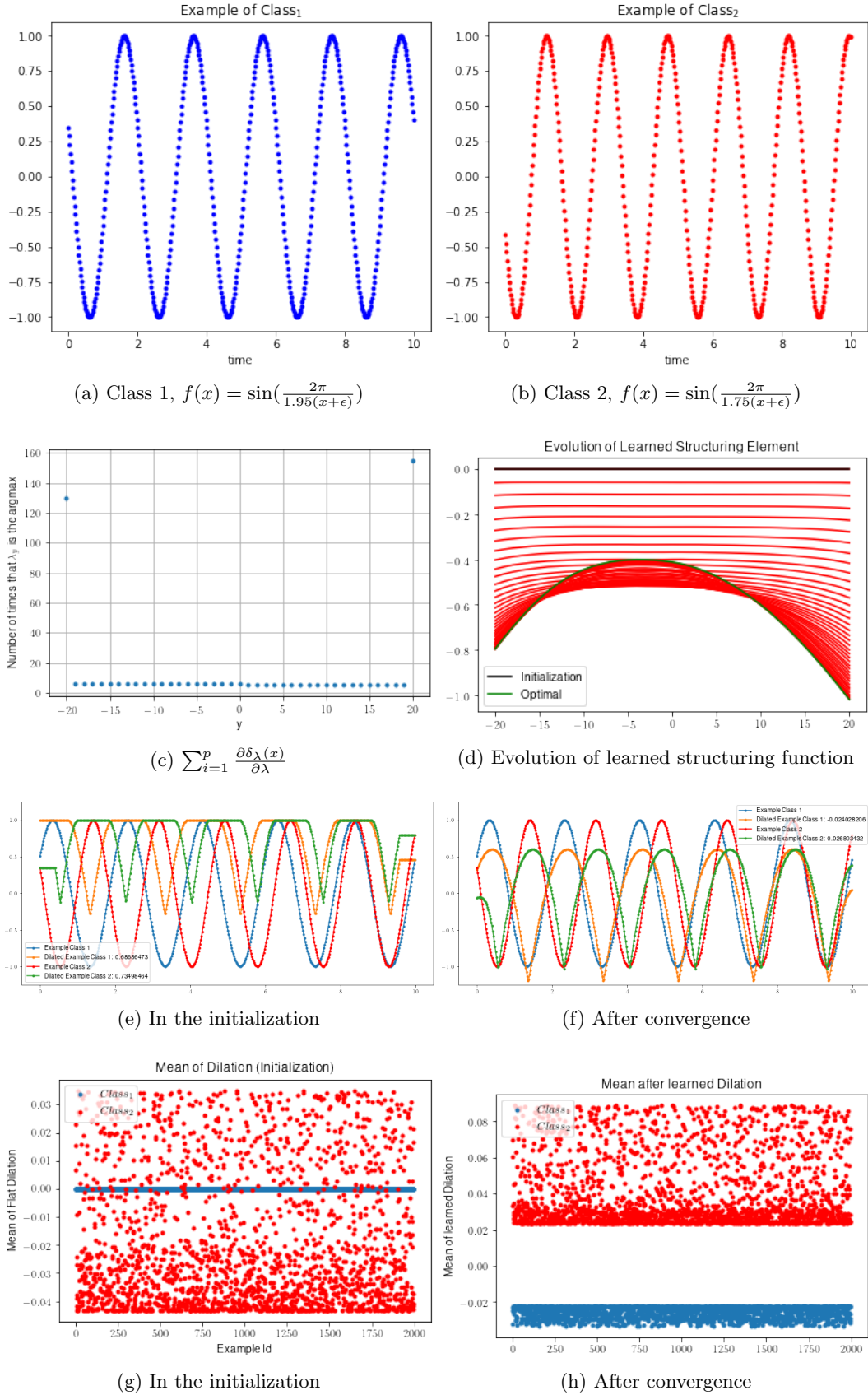


**Figure 5.** Evolution in the case of Nonflat structuring function learning in a classification problem based on dilation and average pooling.

Layer (type)	Output Shape	Param #	Layer (type)	Output Shape	Param #
InputLayer	(None, 103, 1, 1)	0	input (InputLayer)	[(None, 103, 1, 10)]	0
conv2d (Conv2D)	(None, 80, 1, 20)	500	conv2d (Conv2D)	(None, 80, 1, 20)	4820
max_pooling2d	(None, 16, 1, 20)	0	max_pooling2d	(None, 16, 1, 20)	0
flatten	(None, 320)	0	flatten (Flatten)	(None, 320)	0
dense	(None, 100)	32100	dense (Dense)	(None, 100)	32100
batch_normalization	(None, 100)	400	batch_normalization	(None, 100)	400
activation	(None, 100)	0	activation (Activation)	(None, 100)	0
dense_1 (Dense)	(None, 9)	909	dense (Dense)	(None, 9)	909
Total params: 33,909			Total params: 38,229		

**Figure 6.** Baseline architecture vs Baseline architecture applied to EMD. The baseline uses a 20 convolutions 2D with a kernel size of (24,1) followed by a max-pooling reduction of size (5,1) and a RELU activation. For the case presented in the experimental section the same baseline architecture is used. In (b) is the same baseline architecture adapted for ten empirical modes.

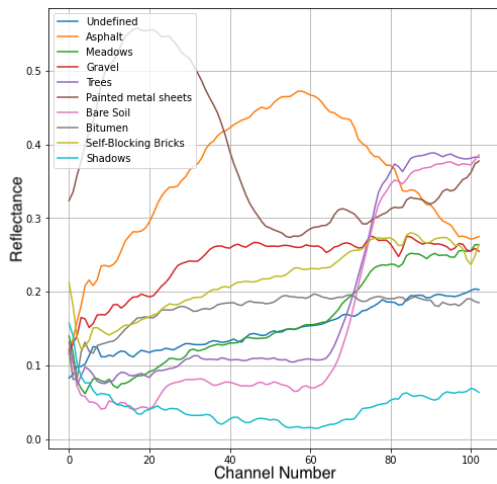
392 **4. Experimental results on hyperspectral classification.** In this section, we investigate  
393 the application of the proposed morphological empirical mode layer (Figure 4) to the problem  
394 of signal classification. In particular, we will focus in the case of supervised classification of  
395 high-dimensional 1D signals in hyperspectral images. The architecture chosen as baseline is  
396 the one recommended in [40] and illustrated in Figure 6. More specifically, the network is  
397 composed of convolution layers, RELU, max-pooling. Each stage consists of twenty convolu-  
398 tion layers with a kernel size of 24 channels followed by ReLU activation, and a dense layer  
399 with batch normalization. In the experimental section, the proposed morphological empirical  
400 mode will be used as the first layer of an architecture of the baseline neural network.

401 **4.1. Considered datasets.** The aim of this section is to compare the results obtained by  
402 different proposed EMD for 1D supervised classification problems. Accordingly, we used as  
403 benchmark two classical hyperspectral images (HIS):

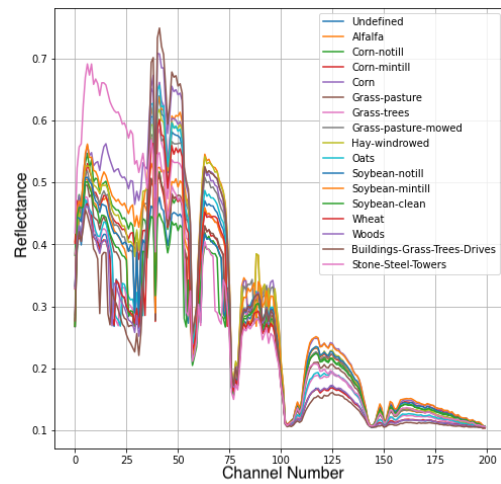
- 404 • *Pavia University* hyperspectral is a scene acquired by the ROSIS sensor in the north  
405 of Italy. The dataset contains nine different classes including multiple solid structures,  
406 natural objects and shadows (Figure 7(a-c)). After discarding the noisy bands, the  
407 considered scene contains 103 spectral bands, with a size of  $610 \times 340$  pixels with  
408 spatial resolution of 1.3 mpp and covering the spectral range from 0.43 to 0.86  $\mu\text{m}$ .
- 409 • *Indian Pines* dataset is a hyperspectral image captured over an agricultural area char-  
410 acterized by its crops of regular geometry and also irregular forest regions. The scene  
411 consists of  $145 \times 145$  pixels and with 224 spectral bands, which have been collected  
412 in the wavelength range from 0.4 to 2.5  $\mu\text{m}$ . There are 16 different classes for train-  
413 ing/testing set with a highly unbalanced distribution (Figure 7(d-f)).

414 **4.1.1. Protocol.** HSI scenes generally suffer from high intraclass variability and interclass  
415 similarity, resulting from uncontrolled phenomena such as variations in illumination, presence  
416 of areas shaded and/or covered by clouds, among others. Accordingly, the selection of training  
417 samples must be carried out very carefully. Deep learning models for HSI have been tradi-  
418 tionally trained by extracting random samples from available ground-truth. However, some  
419 works emphasize that the random sampling strategy has a great influence on the reliability

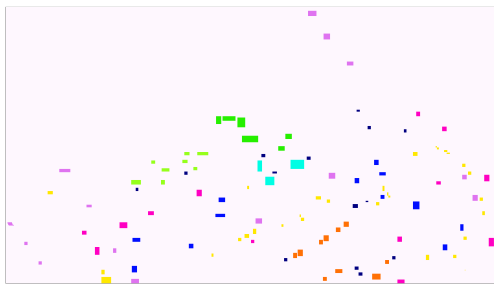




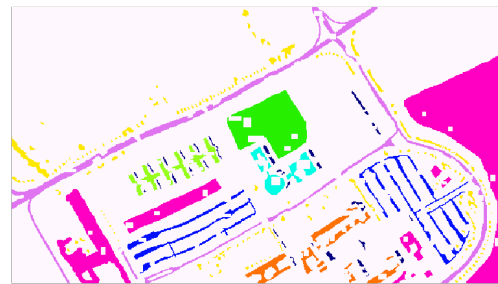
(a) In Pavia University HSI, each data point corresponding to a vector is 103 dimensions. An example per class is shown from the training set in (c).



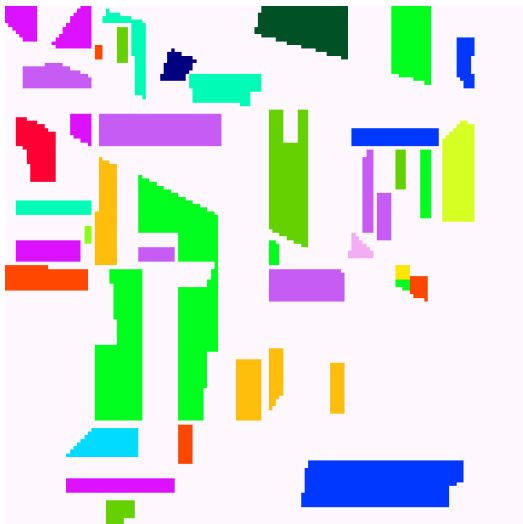
(b) In Indian Pines HSI, each data point corresponds to a vector in 224 dimensions. An example per class is shown from the training set in (e).



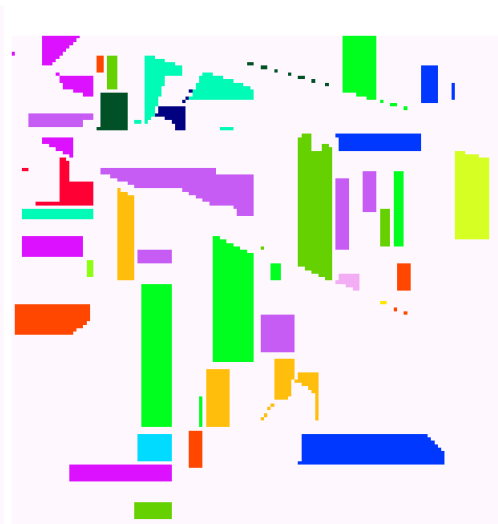
(c) Spatial position of training set in 9 classes for Pavia University HSI.



(d) Spatial position of testing set for Pavia University HSI.



(e) Spatial position of training set in 16 classes for Indian Pines HSI.



(f) Spatial position of testing set for Indian Pines HSI.

**Figure 7.** For considered HSI dataset, (a) an example per class in Pavia University and (b) Indian Pines. Spatial disjoint distribution of training and testing sets: for Pavia University in (c-d) and for Indian Pines in (e-f). In both cases, white pixels are not considered in the evaluation.

420 and the quality of the solution obtained in HSI [40]. In order to avoid this import issue, we  
 421 have follow the recommendation of using *spatial-disjoint samples*, *i.e.*, to have used a strict  
 422 spatial-separation between training and testing sets, allowing us to compare our models in a  
 423 difficult and realist case. The selected training and testing samples have been illustrated in  
 424 [Figure 7\(b-c\)](#) for Pavia University and (e-f) for Indian Pines datasets.

425 In gradient descent approaches the selection of random initialization of the parameter  
 426 value is critical. The aim of this initialization is to prevent layer activation outputs from  
 427 exploding or vanishing during the course of a forward pass [17]. While the source of difficulty  
 428 is well-understood, there is no universal remedy. For our MEM layers, we have used the  
 429 following initialization:

- 430 1. For non-flat structuring functions, a flat structuring element, *i.e.*,  $SE_W$  is a zero matrix.
- 431 2. For quadratic structuring functions,  $\lambda$  is a random realization of a uniform distribution  
 432 between one and four, and for the parameter  $c$ , a uniform distribution between .5 and  
 433 .95.
- 434 3. For the parameter  $\alpha$  in (2.7), the value .5 is used.

435 **4.1.2. Quantitative results.** We explore the use of proposed EMDs as preprocessing lay-  
 436 ers, that means instead of learning the classification task from the original spectral signals,  
 437 we will use the residual of a single step of the decomposition by MEMD. The parameters of  
 438 the MEMD are learned in a gradient-based learning method. As a manner of comparison,  
 439 we report in [Figure 9](#) and [Figure 10](#) the accuracy over testing samples for different proposed  
 440 envelopes by varying both the number of MEM from 10 to 40 and the type of structuring  
 441 function. Each point is the performance for the best model trained from different random ini-  
 442 tialization and an early stopping parameter of ten, *i.e.*, we have stopped the training process if  
 443 it is not improving during ten successive epochs. As it is common in supervised classification  
 444 problems, we have used categorical cross-entropy as loss function. Additionally, for quantita-  
 445 tive comparisons, we have reported best, mean and standard deviation after ten repetitions on  
 446 both Indian Pines HSI ([Table 1](#)) and Pavia University HSI ([Table 2](#)). In general, the following  
 447 results can be highlighted:

- 448 • Learning the parameter in the  $\alpha$ -Morphological Empirical Mode (2.7) improves the  
 449 performance. This can be observed in ([Table 1](#)) and Pavia University HSI ([Table 2](#))  
 450 by comparing the performance of models trained with  $\alpha = 0.5$  and models where  
 451 this parameter is learned. Additionally, in [Figure 9](#) and [Figure 10](#) this fact has been  
 452 highlighted by using different colors in the representation.
- 453 • Quadratic MEMDs perform significantly worse than non-flat ones. However, we would  
 454 like to highlight that the number of parameters is less in the first case.
- 455 • In the considered HSI supervised classification problems, the best of the proposed ap-  
 456 proaches have a performance equivalent to our baseline, which is the state-of-the-art  
 457 for the considered problems ([Table 3](#)). However, we remark that the inclusion of mor-  
 458 phological EMDs induces an invariant to additive intensity shifts in the classification  
 459 model. To illustrate this fact, we have trained a classical model [Figure 6](#) with and  
 460 without a random data augmentation by using an additive shift as transformation.  
 461 That is the usual approach to include some invariance in deep learning models. This  
 462 gives an improvement in the invariance measure in [Figure 8](#). We highlight that by

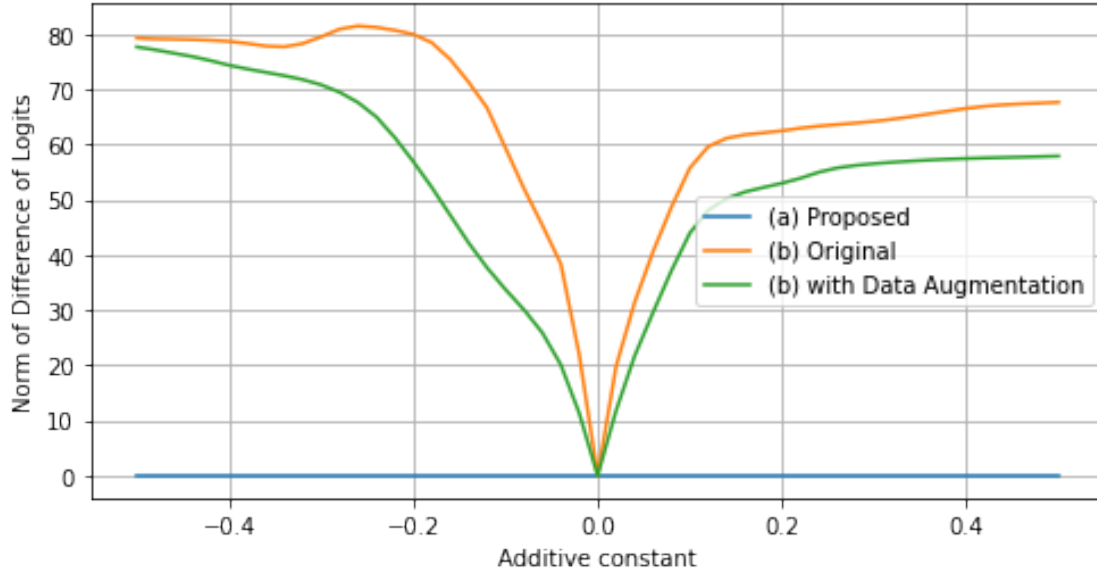


**Figure 8.** Analysis of invariance against additive shift for the training sample of Indian Pines. Norm of the Difference in the predictions with and without additive shift, i.e.,  $\|pred(x) - pred(x + c)\|_2^2$  for different values of  $c$  is given for three models: a) MEMD by  $(\varepsilon, \delta)$ , b) baseline model, c) baseline model with a data augmentation by random additive constant. We highlight that by Remark 2.8 all the MEMD based models are invariant to additive shifts.

463 Remark 2.8 all the MEMD based models are intrinsically invariant to additive shifts,  
 464 which is illustrated in Figure 8.

465 **5. Discussion.** The paper investigated the formulation of EMD based on morphological  
 466 operators and its integration into deep learning architectures. The training of the layers  
 467 realizing the EMD process allows them to adapt the morphological models to the signals to  
 468 be classified. The assessments have been done for supervised classification problem in 1D  
 469 signals from hyperspectral images (*i.e.*, pixelwise spectra), but the proposed approaches are  
 470 applicable to CNN architectures for  $nD$  images, without conceptual or algorithmic problem.  
 471 1D signals have been used for the only reason that the effects of the process on such signals  
 472 are easier to interpret in a research perspective. Several variants of the morphological layers  
 473 have been used. However, we think that for a better understanding of some of the elements of  
 474 the approach: behaviour of the gradient of the layers during the optimization, contribution of  
 475 the different parts of the signals to the optimization, effect of the initialization, etc. a deeper  
 476 theoretical and empirical study is required. Additionally, we have illustrated the use of only  
 477 one decomposition but the presented framework allows us to go further. In the future work,  
 478 we are planning to use some interesting approaches to propose more adapted optimization  
 479 schemes [8] for max-plus based layers, which reveals remarkable properties of network pruning  
 480 by these operators [56]. Additionally, we will explore: a) the use for the MEMD of other  
 481 structuring functions as Poweroids or Anisotropic Quadratic functions as proposed in [47], b)  
 482 to consider the interest of MEMD to produce Scale Equivariant Neural Networks as in [46].

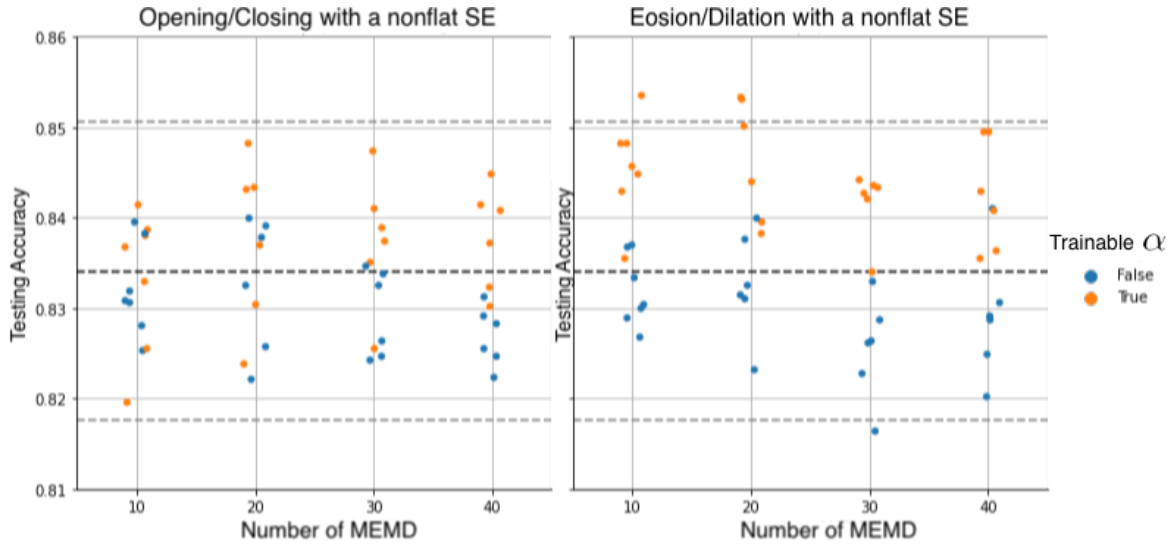


**Figure 9.** Test accuracy for spatial-disjoint samples in Indian Pines Hyperspectral image. Envelopes produces by opening/closing MEMD (left figure) and erosion/dilation MEMD(right figure) by flat structuring function are used in the architecture presented in Figure 6. In both the number of MEMD varies from 10 to 40. Each point is the performance for the best model trained from different random initialization and same early stopping parameter (patience of ten epochs). The horizontal lines indicate the maximum/average/minimum performance of baseline architecture [40] on original data. Blue points correspond to  $\alpha = .5$ , i.e., when this parameter was not learned.

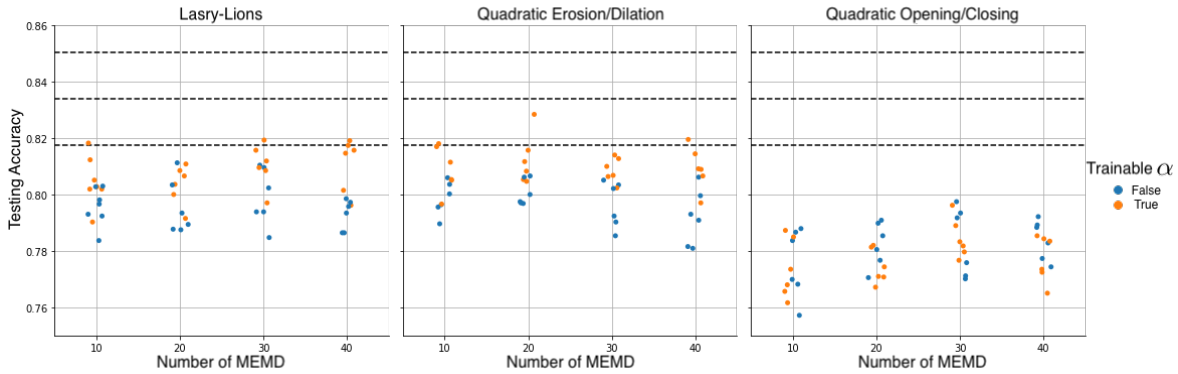


**Figure 10.** Test accuracy for spatial-disjoint samples in Indian Pines Hyperspectral image. Envelopes produces by Lasry-Lions operator (left figure), erosion/dilation (central figure), and opening/closing (right figure) by quadratic structuring functions are used in the architecture presented in Figure 6. The number of MEMD varies from 10 to 40. Each point is the performance for the best model trained from different random initialization and same early stopping parameter (patience of 10 epochs). The horizontal lines indicate the maximum/average/minimum performance of baseline architecture [40] on original data. Blue points correspond to  $\alpha = .5$ , where this parameter was not learned.

Type	Operator	$\alpha$	Overall Val. Acc.		Overall Training Acc.	
			Best	$\mu \pm \sigma$	Best	$\mu \pm \sigma$
Baseline	—	—	85.035	83.929±0.654	93.443	91.413±1.696
NonFlat	$(\gamma, \varphi)$	.5	84.080	83.239 ± 0.512	97.012	95.495±1.184
		True	84.420	83.490 ± 0.656	97.223	96.012 ± 0.847
	$(\varepsilon, \delta)$	.5	83.252	82.764 ± 0.576	97.451	95.226 ± 2.065
		True	<b>85.311</b>	84.052 ± 1.227	95.922	94.015 ± 2.717
	$(\varepsilon, \delta)$ SE(0) $\geq 0$	.5	83.379	82.870 ± 0.261	96.889	95.621 ± 1.043
		True	85.247	83.821 ± 0.787	96.168	0.94874 ± 1.120
Quadratic	$(\gamma, \varphi)$	.5	79.495	78.024 ± 0.754	96.080	93.580 ± 2.625
		True	80.959	77.971 ± 1.563	97.645	95.043 ± 1.565
	$(\varepsilon, \delta)$	.5	81.363	79.798 ± 1.006	96.484	94.964± 1.111
		True	81.596	80.847 ± 0.537	97.223	95.066± 1.191
	Lasry-Lions	.5	81.384	79.909 ± 0.876	96.924	95.273 ± 1.336
		True	82.424	81.299 ± 0.983	96.941	95.674 ± 0.927

Table 1

Experiment on hyperspectral Indian Pines Disjoint classification problem. Each experiment has been repeated ten times varying the initialization of base architecture. Twenty filters of MEMD in a single level of simplification. The training was performed without any data augmentation technique. The constraint  $SE(0) \geq 0$  is used to assure the order relation among envelopes (See Remark 1.2)

Type	Operator	$\alpha$	Overall Val. Acc.		Overall Training Acc.	
			Best	$\mu \pm \sigma$	Best	$\mu \pm \sigma$
Baseline	—	—	85.468	83.396± 2.420	92.527	86.447 ± 8.960
NonFlat	$(\gamma, \varphi)$	.5	79.543	78.189 ± 0.726	95.715	92.219 ± 2.408
		True	82.353	79.293 ± 1.767	96.353	91.525 ± 4.335
	$(\varepsilon, \delta)$	.5	84.261	82.681 ± 0.798	93.726	88.794 ± 4.998
		True	84.133	82.529 ± 1.131	93.879	89.735 ± 2.118
	$(\varepsilon, \delta)$ , SE(0) $\geq 0$	.5	83.908	81.740 ± 1.295	93.216	84.575 ± 7.334
		True	<b>85.483</b>	83.994 ± 1.238	94.389	89.617 ± 3.289
Quadratic	$(\gamma, \varphi)$	.5	74.516	70.821 ± 2.023	91.201	80.951 ± 6.432
		True	73.539	69.399 ± 2.339	93.828	87.360 ± 6.443
	$(\varepsilon, \delta)$	.5	77.411	75.432 ± 1.193	95.052	86.470 ± 5.939
		True	81.196	77.923 ± 1.700	92.476	86.593 ± 6.585
	Lasry-Lions	.5	77.461	76.396 ± 0.614	97.067	90.826 ± 6.223
		True	80.971	78.501 ± 1.332	96.123	87.082 ± 8.221

Table 2

Experiment on hyperspectral Pavia University for a disjoint training sample. Nine different classes. Each experiment has been repeated ten times varying the initialization of base architecture. Twenty filters of MEMD in a single level of simplification. The training was performed without any data augmentation technique. The constraint  $SE(0) \geq 0$  is used to assure the order relation among envelopes (See Remark 1.2)

Method	Indian Pines	Pavia University
Random Forest	65.79	69.64
Multinomial Logistic regression	83.81	72.23
Support Vector Machines	85.08	77.80
MLP	83.81	81.96
CNN1D	85.03	85.47
$\Phi_{\varepsilon,\delta}^\alpha$ + CNN1D	85.31	85.48

Table 3

Comparison (in terms of OA) between different HSI classification models trained on spatial-disjoint samples. The performance for first four models are included for comparison from [40].

483 Finally, we highlight that the study of theoretical properties of morphological networks in the  
 484 sense of their *expressiveness and universality* [57] is fundamental to have a full understanding  
 485 of the limits of these types of layers when they are integrated in DL architectures.

486 **Acknowledgments.** This work has been supported by *Fondation Mathématique Jacques*  
 487 *Hadamard* (FMJH) under the PGMO-IRSDI 2019 program. This work was granted access to  
 488 the Jean Zay supercomputer under the allocation 2020- AD011012212.

## REFERENCES

- 489
- 490 [1] J. ANGULO, *Lipschitz Regularization of Images supported on Surfaces using Riemannian Morphological*  
 491 *Operators*. Preprint, Nov. 2014, <https://hal-mines-paristech.archives-ouvertes.fr/hal-01108130>.
- 492 [2] J. ANGULO AND S. VELASCO-FORERO, *Riemannian mathematical morphology*, *Pattern Recognition Let-*  
 493 *ters*, 47 (2014), pp. 93–101.
- 494 [3] J. BEDI AND D. TOSHNIWAL, *Empirical mode decomposition based deep learning for electricity demand*  
 495 *forecasting*, *Ieee Access*, 6 (2018), pp. 49144–49156.
- 496 [4] Y. BENGIO, Y. LECUN, AND H. HINTON, *Deep learning*, *Nature*, 521 (2015), pp. 436–444.
- 497 [5] J. BOSWORTH AND S. T. ACTON, *The morphological lomo filter for multiscale image processing*, in *Pro-*  
 498 *ceedings 1999 International Conference on Image Processing (Cat. 99CH36348)*, vol. 4, IEEE, 1999,  
 499 pp. 157–161.
- 500 [6] Y.-L. BOUREAU, J. PONCE, AND Y. LECUN, *A theoretical analysis of feature pooling in visual recognition*,  
 501 in *ICML 2010*, 2010, pp. 111–118.
- 502 [7] M. CARLSSON, *On convex envelopes and regularization of non-convex functionals without moving global*  
 503 *minima*, *Journal of Optimization Theory and Applications*, 183 (2019), pp. 66–84.
- 504 [8] V. CHARISOPOULOS AND P. MARAGOS, *Morphological perceptrons: Geometry and training algorithms*, in  
 505 *Mathematical Morphology and Its Applications to Signal and Image Processing*, Springer Interna-  
 506 tional Publishing, 2017, pp. 3–15.
- 507 [9] J. CHEN, X. WANG, AND C. PLANIDEN, *A proximal average for prox-bounded functions*, *SIAM Journal*  
 508 *on Optimization*, 30 (2020), pp. 1366–1390.
- 509 [10] E. DELÉCHELLE, J. LEMOINE, AND O. NIANG, *Empirical mode decomposition: an analytical approach for*  
 510 *sifting process*, *IEEE Signal Processing Letters*, 12 (2005), pp. 764–767.
- 511 [11] E. H. S. DIOP AND R. ALEXANDRE, *Analysis of intrinsic mode functions based on curvature motion-like*  
 512 *pdes*, in *Curves and Surfaces*, J.-D. Boissonnat, A. Cohen, O. Gibaru, C. Gout, T. Lyche, M.-L.  
 513 Mazure, and L. L. Schumaker, eds., Cham, 2015, Springer International Publishing, pp. 202–209.
- 514 [12] E. H. S. DIOP, R. ALEXANDRE, AND L. MOISAN, *Intrinsic nonlinear multiscale image decomposition: A*  
 515 *2D empirical mode decomposition-like tool*, *Computer Vision and Image Understanding*, 116 (2012),  
 516 pp. 102–119. *Virtual Representations and Modeling of Large-scale Environments (VRML)*.
- 517 [13] R. A. E.-H. S. DIOP AND V. PERRIER, *A PDE model for 2d intrinsic mode functions*, *IEEE ICIP*, (2009).

- 518 [14] G. FRANCHI, A. FEHRI, AND A. YAO, *Deep morphological networks*, Pattern Recognition, 102 (2020),  
519 p. 107246.
- 520 [15] J. GILLES, *Empirical wavelet transform*, IEEE Transactions on Signal Processing, 61 (2013), pp. 3999–  
521 4010.
- 522 [16] J. GOUTSIAS AND H. HEIJMANS, *Mathematical Morphology*, IOS Press, 2000.
- 523 [17] B. HANIN AND D. ROLNICK, *How to start training: The effect of initialization and architecture*, in  
524 Advances in Neural Information Processing Systems, 2018, pp. 571–581.
- 525 [18] K. HE, X. ZHANG, S. REN, AND J. SUN, *Deep residual learning for image recognition*, in Proceedings of  
526 the IEEE conference on Computer Vision and Pattern Recognition, 2016, pp. 770–778.
- 527 [19] Z. HE, J. LI, L. LIU, AND Y. SHEN, *Three-dimensional empirical mode decomposition (TEMD): A fast*  
528 *approach motivated by separable filters*, Signal Processing, 131 (2017), pp. 307–319.
- 529 [20] H. J. HEIJMANS AND P. MARAGOS, *Lattice calculus of the morphological slope transform*, Signal Process-  
530 ing, 59 (1997), pp. 17–42.
- 531 [21] H. J. HEIJMANS AND C. RONSE, *The algebraic basis of mathematical morphology i. dilations and erosions*,  
532 Computer Vision, Graphics, and Image Processing, 50 (1990), pp. 245–295.
- 533 [22] H. J. HEIJMANS AND R. VAN DEN BOOMGAARD, *Algebraic framework for linear and morphological scale-*  
534 *spaces*, Journal of Visual Communication and Image Representation, 13 (2002), pp. 269–301.
- 535 [23] T. Y. HOU AND Z. SHI, *Adaptive data analysis via sparse time-frequency representation*, Advances in  
536 Adaptive Data Analysis, 3 (2011), pp. 1–28.
- 537 [24] N. HUANG, S. ZHENG, S. LONG, M. WU, H. SHIH, Q. ZHENG, N.-C. YEN, C. TUNG, AND H. LIU, *The*  
538 *empirical mode decomposition and the Hilbert spectrum for nonlinear and non-stationary time series*  
539 *analysis*, The Royal Society, 454 (1998), pp. 903–995.
- 540 [25] P. T. JACKWAY, *Morphological scale-spaces*, in Advances in Imaging and Electron Physics, P. W. Hawkes,  
541 ed., vol. 99, Elsevier, 1997, pp. 1–64.
- 542 [26] P. T. JACKWAY AND M. DERICHE, *Scale-space properties of the multiscale morphological dilation-erosion*,  
543 IEEE Transactions on Pattern Analysis and Machine Intelligence, 18 (1996), pp. 38–51.
- 544 [27] X.-B. JIN, N.-X. YANG, X.-Y. WANG, Y.-T. BAI, T.-L. SU, AND J.-L. KONG, *Deep hybrid model*  
545 *based on emd with classification by frequency characteristics for long-term air quality prediction*,  
546 Mathematics, 8 (2020), p. 214.
- 547 [28] P.-L. L. J.M. LASRY, *A remark on regularization in Hilbert spaces*, Israel Journal of Mathematics, 55  
548 (1986), pp. 257–266.
- 549 [29] A. KIRSZENBERG, G. TOCHON, É. PUYBAREAU, AND J. ANGULO, *Going beyond p-convolutions to learn*  
550 *grayscale morphological operators*, in Discrete Geometry and Mathematical Morphology, J. Lindblad,  
551 F. Malmberg, and N. Sladoje, eds., Cham, 2021, Springer International Publishing, pp. 470–482.
- 552 [30] D. LOONEY AND D. P. MANDIC, *A machine learning enhanced empirical mode decomposition*, in IEEE  
553 ICASSP, IEEE, 2008, pp. 1897–1900.
- 554 [31] P. MARAGOS, *Representations for morphological image operators and analogies with linear operators*,  
555 Advances in imaging and electron physics, 177 (2013), pp. 45–187.
- 556 [32] P. MARAGOS, J. F. KAISER, AND T. F. QUATIERI, *Energy separation in signal modulations with appli-*  
557 *cation to speech analysis*, IEEE Transactions on Signal Processing, 41 (1993), pp. 3024–3051.
- 558 [33] J. MASCI, J. ANGULO, AND J. SCHMIDHUBER, *A learning framework for morphological operators using*  
559 *counter-harmonic mean*, in Mathematical Morphology and Its Applications to Signal and Image  
560 Processing, Springer, 2013, pp. 329–340.
- 561 [34] R. MONDAL, M. S. DEY, AND B. CHANDA, *Image restoration by learning morphological opening-closing*  
562 *network*, Mathematical Morphology - Theory and Applications, 4 (01 Jan. 2020), pp. 87 – 107.
- 563 [35] J.-J. MOREAU, *Proximité et dualité dans un espace hilbertien*, Bulletin de la Société mathématique de  
564 France, 93 (1965), pp. 273–299.
- 565 [36] J. J. MOREAU, *Inf-convolution, sous-additivité, convexité des fonctions numériques*, Journal de  
566 Mathématiques Pures et Appliquées, (1970).
- 567 [37] M. NAKASHIZUKA, *Image regularization with higher-order morphological gradients*, in 2015 23rd European  
568 Signal Processing Conference (EUSIPCO), IEEE, 2015, pp. 1820–1824.
- 569 [38] K. NOGUEIRA, J. CHANUSSOT, M. D. MURA, W. R. SCHWARTZ, AND J. A. DOS SANTOS, *An introduction*  
570 *to deep morphological networks*, 2019, <https://arxiv.org/abs/1906.01751>.
- 571 [39] S. J. NOWLAN AND G. E. HINTON, *Simplifying neural networks by soft weight-sharing*, Neural computa-

- 572 tion, 4 (1992), pp. 473–493.
- 573 [40] M. PAOLETTI, J. HAUT, J. PLAZA, AND A. PLAZA, *Deep learning classifiers for hyperspectral imaging:*  
574 *A review*, ISPRS Journal of Photogrammetry and Remote Sensing, 158 (2019), pp. 279–317.
- 575 [41] N. PARIKH AND S. BOYD, *Proximal algorithms*, Foundations and Trends in optimization, 1 (2014),  
576 pp. 127–239.
- 577 [42] L. F. PESSOA AND P. MARAGOS, *MRL-filters: A general class of nonlinear systems and their optimal*  
578 *design for image processing*, IEEE Transactions on Image Processing, 7 (1998), pp. 966–978.
- 579 [43] X. QIU, Y. REN, P. N. SUGANTHAN, AND G. A. AMARATUNGA, *Empirical mode decomposition based*  
580 *ensemble deep learning for load demand time series forecasting*, Applied Soft Computing, 54 (2017),  
581 pp. 246–255.
- 582 [44] R. T. ROCKAFELLAR AND R. J.-B. WETS, *Variational analysis*, vol. 317, Springer Science & Business  
583 Media, 2009.
- 584 [45] R. ROJAS, *The backpropagation algorithm*, in Neural networks, Springer, 1996, pp. 149–182.
- 585 [46] M. SANGALLI, S. BLUSSEAU, S. VELASCO-FORERO, AND J. ANGULO, *Scale equivariant neural networks*  
586 *with morphological scale-spaces*, in Discrete Geometry and Mathematical Morphology, J. Lindblad,  
587 F. Malmberg, and N. Sladoje, eds., Cham, 2021, Springer International Publishing, pp. 483–495.
- 588 [47] M. SCHMIDT AND J. WEICKERT, *Morphological counterparts of linear shift-invariant scale-spaces*, Journal  
589 of Mathematical Imaging and Vision, 56 (2016), pp. 352–366.
- 590 [48] J. SERRA, *Image Analysis and Mathematical Morphology*, Academic Press, Inc., Orlando, FL, USA, 1983.
- 591 [49] R. C. SHARPLEY AND V. VATCHEV, *Analysis of the intrinsic mode functions*, Constructive Approximation,  
592 24 (2006), pp. 17–47.
- 593 [50] S. SINCLAIR AND G. PEGRAM, *Empirical mode decomposition in 2-d space and time: a tool for space-time*  
594 *rainfall analysis and nowcasting*, Hydrology and Earth System Sciences, 9 (2005), pp. 127–137.
- 595 [51] A. STALLONE, A. CICONE, AND M. MATERASSI, *New insights and best practices for the successful use of*  
596 *empirical mode decomposition, iterative filtering and derived algorithms*, Scientific reports, 10 (2020),  
597 pp. 1–15.
- 598 [52] R. VAN DEN BOOMGAARD, L. DORST, S. MAKRAM-EBEID, AND J. SCHAVEMAKER, *Quadratic structuring*  
599 *functions in mathematical morphology*, in Mathematical morphology and its applications to image and  
600 signal processing, Springer, 1996, pp. 147–154.
- 601 [53] R. VAN DEN BOOMGAARD AND A. SMEULDERS, *The morphological structure of images: The differential*  
602 *equations of morphological scale-space*, IEEE Transactions on Pattern Analysis and Machine Intelli-  
603 gence, 16 (1994), pp. 1101–1113.
- 604 [54] L. J. VAN VLIET, I. T. YOUNG, AND G. L. BECKERS, *A nonlinear Laplace operator as edge detector in*  
605 *noisy images*, Computer Vision, Graphics, and Image Processing, 45 (1989), pp. 167 – 195.
- 606 [55] S. VELASCO-FORERO AND J. ANGULO, *On nonlocal mathematical morphology*, in International Sympo-  
607 sium on Mathematical Morphology and Its Applications to Signal and Image Processing, Springer,  
608 2013, pp. 219–230.
- 609 [56] Y. ZHANG, S. BLUSSEAU, S. VELASCO-FORERO, I. BLOCH, AND J. ANGULO, *Max-plus operators ap-*  
610 *plied to filter selection and model pruning in neural networks*, in Mathematical Morphology and Its  
611 Applications to Signal and Image Processing, Springer International Publishing, 2019, pp. 310–322.
- 612 [57] D.-X. ZHOU, *Universality of deep convolutional neural networks*, Applied and computational harmonic  
613 analysis, 48 (2020), pp. 787–794.